Spatial population structure determines extinction risk in climate-induced range shifts

Manuscript elements: Figure 1, figure 2, figure 3, online appendices A and B (including figures A1-A3, tables A1-A4, and figures B1-B11). Figure 1 and figure 3 are to print in color.

Keywords: range shifts, extinction, rapid evolution, dispersal evolution, individual-based model

Manuscript type: Article.

Abstract

Climate change is an escalating threat facing populations around the globe, necessitating a robust understanding of the ecological and evolutionary mechanisms dictating population responses. However, populations do not respond to climate change in isolation, but rather in the context of their existing ranges. In particular, spatial population structure within a range (e.g. trait clines, starkness of range edges, etc.) likely interacts with other ecological and evolutionary processes during climate-induced range shifts. Here, we use an individual-based model to explore the interacting roles of these factors in range shift dynamics. We show that increased spatial population structure (driven primarily by a steeper slope in the trait optimum gradient) severely increased a population's extinction risk. Further, and contrary to expectations, we show that evolution of heightened dispersal during range shifts was unable to rescue faltering populations. Rather, a population's fate during climate change was determined by the composition of dispersal phenotypes defining the population at equilibrium (i.e. before the onset of rapid climate change); only populations consisting of highly dispersive individuals survived. Our results demonstrate that dispersal evolution alone may be insufficient to save a range shifting population and that spatial population structure can substantially increase extinction risk in range shifts.

Introduction

Climate change is expected to dramatically reshape global biogeographic patterns as some species shift their ranges to track changing environmental conditions (Gonzalez et al., 2010). These range shifts are generally predicted to proceed upwards in latitude, elevation, or both as average global temperatures continue to rise (Loarie et al., 2009). Indeed, contemporary range shifts have already been observed in a wide variety of taxa, from algae to mammals (Chen et al., 2011; Parmesan, 2006). Such range shifts present significant challenges to current and future conservation efforts as they can result in the extinction of populations failing to track a changing climate (Parmesan, 2006) as well as the creation of novel species assemblages (Hobbs et al., 2009). Understanding the ecological and evolutionary dynamics of such climate-induced range shifts will play a key role in informing current and future conservation work.

Large-scale population movements have been studied for decades in the context of range expansions (e.g. of invasive or reintroduced species), leading to a robust understanding of both the ecological (Hastings et al., 2005) and evolutionary (Excoffier et al., 2009; Shine et al., 2011) mechanisms shaping such expansions. For example, while the speed of a range expansion can be well approximated by a combination of the species' intrinsic growth rate and dispersal ability (Fisher, 1937; Hastings et al., 2005), recent research demonstrates that evolution in both of these traits can increase both the mean and variance of expansion speed through time (Ochocki and Miller, 2017; Phillips, 2015; Shaw and Kokko, 2015; Szűcs et al., 2017; Weiss-Lehman et al., 2017). As fundamentally similar spatial processes, it is likely that range shifts will also be subject to the same ecological and evolutionary mechanisms known to drive range expansions. However, range shifts involve several additional complications absent from range expansions, which must be considered when predicting the dynamics of a shifting population. In particular, range shifts begin

with far more complex spatial population structure compared to most range expansions. Here and throughout the paper, we use the phrase "spatial population structure" to refer broadly to the spatial distribution of individuals, and their associated genotypes and phenotypes, within a population. Thus, spatial population structure can encompass factors such as spatial clines in trait values and the starkness of abundance declines characterizing the range edge. Range expansions (e.g. of invasive or reintroduced species) typically start from small founding populations brought to a new area and lacking any initial spatial population structure. While such populations form spatial population structure during the expansion process (Ochocki and Miller, 2017; Weiss-Lehman et al., 2017), established populations respond to climate change in the context of preexisting spatial population structure.

Each factor relating to spatial population structure has the potential to affect the dynamics of range shifts under changing climatic conditions. For example, the underlying mechanism causing population declines at the range edge (e.g. declines in carrying capacity versus growth rate) can alter a population's extinction risk during climate driven range shifts (Henry et al., 2013). Further, in ranges characterized by a gradient in a trait optimum, the starkness of the range edge can impact the ability of peripheral populations to adapt to the local optimum, with stark range edges leading to better adaptation in peripheral populations (García-Ramos and Kirkpatrick, 1997), though the importance of this for range shifts has not been investigated. Additionally, the nature of dispersal can interact with adaptation to a trait optimum gradient to impact range shift dynamics. When dispersal occurs in a stepping stone manner, maladapted individuals (i.e. individuals whose phenotypes do not match the local optimum) can block the establishment of better adapted genotypes so long as the mismatch is not too severe (Atkins and Travis, 2010). While these aspects of spatial population structure have been shown to impact the dynamics of climate-induced range shifts in isolation, it is unclear how and if they might interact.

4

Further, given the importance of rapid trait evolution in range expansions (Ochocki and Miller, 2017; Phillips, 2015; Shaw and Kokko, 2015; Szűcs et al., 2017; Weiss-Lehman et al., 2017), it is necessary to consider the interplay between aspects of spatial population structure and the role of rapid evolution during range shifts. In asexual species, for example, local adaptation to a trait optimum gradient has been shown to interact with dispersal evolution during climate change, driving increased dispersal probability as genotypes shift to keep pace with their environmental optimum (Hargreaves et al., 2015). However, it is unclear how these two processes might interact in a sexually reproducing species in which dispersal and local adaptation are directly linked via gene flow. Under sexual reproduction, evolution of increased dispersal could simultaneously reduce local adaptation to a trait optimum gradient within a population due to increased gene flow throughout the range (García-Ramos and Kirkpatrick, 1997; Kirkpatrick and Barton, 1997). In fact, long-distance pollen dispersal in flowering plants has been shown to restrict local adaptation and, when pollen dispersal sufficiently outpaces seed dispersal, to lead to ecological niche shifts, rather than spatial range shifts, in response to simulated climate change (Aguilée et al., 2016). In addition to potential interactions between local adaptation and dispersal evolution, the starkness of the range edge could influence the potential for rapid trait evolution during range shifts by altering the spatial distribution of dispersal phenotypes throughout the range (Hargreaves and Eckert, 2014; Henry et al., 2013), thus altering the diversity of dispersal genotypes present for subsequent evolution during range shifts.

Here, we assess the interaction of two mechanisms responsible for spatial population structure with trait evolution in sexually reproducing populations undergoing range shifts. We develop an individual-based model capable of producing a wide variety of spatial population structures in which males and females are defined by two genetically determined traits, thus allowing for both evolutionary and ecological responses to climate change. One trait determines dispersal ability

5

while the second defines an individual's environmental niche. Using this model, we vary both the severity of the niche optimum gradient and the starkness of the range edge to ascertain how they interact with each other and with the process of trait evolution to impact a population's ability to track a changing climate. Additionally, by contrasting the dynamics of extant and extinct populations, we isolate the factors most strongly contributing to extinction risk during climate change.

Methods

A full description of the individual-based model using the Overview, Design concepts, and Details protocol (Grimm et al., 2010) is available in Appendix A, while we present a brief summary here. Population dynamics occurred within discrete habitat patches embedded in a two dimensional lattice in which environmental conditions varied along the x dimension but remained constant along the y dimension (Fig. A1). Landscapes were unbounded in the x dimension but defined by a fixed width and wrapping boundaries in the y dimension. The optimum environmental niche value changed linearly along the x dimension, thus allowing for the intrinsic formation of stable range boundaries when the optimum changed rapidly enough (Alleaume-Benharira et al., 2006; Kirkpatrick and Barton, 1997; Polechova, 2018; Polechová and Barton, 2015). However, to examine the dynamics of ranges in which the niche optimum did not change rapidly enough to form stable range limits, we additionally imposed extrinsic range limits to prevent continuous adaptation and spread of the population (Alleaume-Benharira et al., 2006; García-Ramos and Kirkpatrick, 1997). Specifically, we systematically altered the decline in patch carrying capacities from the range core to the edge (Alleaume-Benharira et al., 2006; Bocedi et al., 2014; Henry et al., 2013; Mustin et al., 2009) in such a way that we could directly manipulate the starkness of the decline. Previous research has shown that using a decline in intrinsic growth rate as opposed to carrying capacity may impact extinction risk but does not alter the patterns of dispersal evolution during cli-

6

mate change (Henry et al., 2013). To maintain generality, we do not assume a specific mechanism behind the decline in carrying capacity, but it could represent a variety of range limiting mechanisms such as physiological limits to adaptation, the effects of competition, or underlying resource distributions (Case and Taper, 2000; Holt et al., 2005; Sexton et al., 2009). Thus, the x dimension defined the environmental context of the population and the y dimension allowed for variation in population dynamics under identical environmental conditions. To simulate climate change, the patch carrying capacities and the niche optimum gradient shifted at a constant rate along the x dimension. Generations were non-overlapping and consisted of discrete dispersal and reproduction phases (Fig. A2).

Individuals were characterized by two traits (dispersal and an environmental niche), each defined by a set of 5 quantitative diploid loci. While the number of loci was arbitrary, 5 was chosen as a compromise between computational restrictions and the likely polygenic nature of such complex traits. The dispersal trait defined an individual's expected dispersal distance, assuming an exponential dispersal kernel. An individual's realized dispersal distance was then drawn from the dispersal kernel and dispersal direction was random and unbiased. Dispersal occurred in continuous space from the center of an individual's current patch and the individual's new patch was then determined by the mapping from continuous space to discrete patches (see Appendix A). An individual's environmental niche value determined its fitness according to the local niche optimum. The closer an individual's niche value to the local optimum, the higher the individual's realized fitness. Reproduction within each patch occurred via a stochastic implementation of the classic Ricker model (Melbourne and Hastings, 2008; Ricker, 1954), scaled by the mean fitness of the patch. Parental pairs formed via random sampling of the local population (with replacement) weighted by individual fitness such that individuals with a close match of their niche value to the local optimum produced more offspring on average. Thus, the model used a mixture of hard

7

selection (realized population growth declined with maladaptation relative to the niche optimum) and soft selection (probability of producing offspring depended on fitness relative to other individuals) for the evolutionary dynamics (Wallace, 1975). Allele inheritance was subject to mutation and assumed no linkages among loci. The mutation process was designed such that mutational input per generation was independent of the number of loci (see Appendix A) and with parameters corresponding to previous estimates from the literature (Gilbert et al., 2017).

We varied parameter values to explore the interacting roles of the slope of the niche optimum gradient and range edge starkness (Table A2) in forming spatial population structure at equilibrium and driving the subsequent eco-evolutionary dynamics of range shifts. Specifically, we considered a fully factorial combination of: (1) a flat, shallow, and steep niche optimum gradient, (2) shallow, moderate, and stark declines in carrying capacity at the range edge, and (3) slow, moderate, and fast speeds of climate change. This yielded a total of 27 different scenarios, each explored with 200 simulations. Each simulation ran for 2150 generations with stable climate conditions for the first 2000 to reach a spatial equilibrium, followed by 100 generations of climate change and a final 50 generations of stable conditions. Figure 1 shows an example of a single population responding to a moderate speed of climate change. For each scenario, we evaluated the role of the equilibrium spatial population structure and dispersal evolution in the dynamics of the range shifting populations. We primarily discuss simulations assuming a moderate speed of climate change in the main text, but present the results for slow and fast speeds of climate change in Appendix B.

We calculated dispersal evolution in each patch throughout the landscape as the change in mean dispersal phenotype from the beginning of the period of climate change to the end. For this analysis, we defined individual patches by their relative location within the range rather than with their fixed spatial coordinates (e.g. leading edge vs. core populations). Due to local extinctions, not all patches were occupied at the end of the period of climate change. To quantify dispersal

8

evolution in these patches, we used data from the last generation in which the population had at least 10 individuals. Changes in mean dispersal phenotype were calculated by subtracting the initial mean dispersal phenotype from the value at the end of climate change (or at the last generation of at least 10 individuals occupying the patch in the case of population extinctions); positive values indicate an increase in the mean dispersal phenotype. All simulations and data processing were performed in R version 3.4.4 (Team, 2000) and the code is available at (links are available from the journal office).

Results

In all scenarios, some populations shifted their ranges in response to climate change. However, the proportion of populations that failed to track the changing climate (and subsequently went extinct) depended on the spatial characteristics of the range. Populations defined by a steep niche optimum gradient and by stark declines in carrying capacity at the range edge experienced the greatest probability of extinction due to climate change (quantified by the proportion of simulated populations to go extinct through time; Fig. 2). While both aspects of a population's range influenced extinction probabilities, the niche optimum gradient drove more dramatic changes to extinction risk, with steeper gradients causing severe increases in the probability of extinction during climate change. We varied both parameters widely, doubling the slope of the niche optimum gradient from the shallow to steep scenario and increasing the parameter defining range edge starkness by a factor of 100 from shallow to stark edges (Table A2). This suggests that the niche optimum gradient may be the stronger driver of extinction risk during climate-induced range shifts across a wide region of parameter space and corresponding biological scenarios. Additionally, as expected, the pace of climate change also influenced extinction probabilities with faster climate change corresponding to greater extinction risk (Fig. B1 & B2). However, this effect was independent of the niche optimum

9

gradient and range edge starkness in determining extinction probability during range shifts.

183   In accordance with previous results (García-Ramos and Kirkpatrick, 1997), populations at the range edge had lower fitness than central populations at equilibrium and this effect was amplified with more gradual range edges. Counterintuitively, populations that survived climate change

186   tended to be characterized by even greater reductions in fitness at the range edges at equilibrium compared to populations that went extinct (Fig. B3-B5). While discernible in all simulations with a non-zero slope in the niche optimum gradient, this pattern was most evident in the scenarios de-

189   fined by a gradual range edge. As expected, there was no spatial variation in fitness for populations with no variation in the niche optimum across space. Despite the spatial variation in fitness in some scenarios, variance in relative fitness within a patch was relatively low (about 0.3 across all

192   scenarios). This implies that (1) the reduction in fitness at the edge caused by the niche optimum gradient was relatively uniform across all individuals, and (2) as a result, there was relatively low variance in reproductive success in these populations, meaning that evolution at the edge was not

195   driven by only a handful of higher fitness individuals.

Dispersal evolution is predicted to play a key role in aiding populations as they shift to track a changing climate. While some individual simulations confirmed these expectations with average

198   dispersal phenotypes increasing through time (e.g. Fig. 1), examining all simulations from each experimental scenario revealed no differences in the magnitude or direction of dispersal evolution between successful and extinct populations (Fig. 3a&b). Populations in all parameter combinations

201   experienced both increases and decreases in average dispersal phenotypes, with all distributions of observed changes in dispersal phenotypes centered on 0 (Fig. B3-B5). Further, calculating the coefficient of variation (CV) in dispersal genotypes over the y dimension, in which environmental

204   conditions did not vary, revealed that edge populations had between 3 and 4 times higher CVs than core populations across all scenarios, indicating genetic diversity at the edge was not a limiting

10

factor in dispersal evolution. The similarity in evolved changes in dispersal between surviving

and extinct populations suggests that dispersal evolution alone cannot explain which populations

successfully tracked moving conditions and which became extinct.

Instead, the distribution of dispersal phenotypes at equilibrium played a key role in determining a population's fate. A range of dispersal phenotypes evolved in populations over the 2000 generations of stable climatic conditions in response to the niche optimum gradient and range edge starkness (Fig. B9-B11). Populations that survived climate change were composed primarily of individuals with heightened dispersal phenotypes (Fig. 3c&d). Previous research has demonstrated that defining the range edges via a decline in the intrinsic growth rate (as opposed to carrying capacity as done here) resulted in less dispersive phenotypes at the range edge (Henry et al., 2013), meaning extinction risks would be even higher under such a scenario. Comparing the full distribution of equilibrium dispersal phenotypes present in a given experimental scenario to the distribution of phenotypes just from surviving populations revealed a threshold value delineating individuals from surviving versus extinct populations. Comparison of the different experimental scenarios revealed this threshold to be constant for a given speed of climate change (Fig. B9-B11). To explain this phenomenon, we used the well-known approximation for the speed of an expanding population, $2\sqrt{rD}$ (Fisher, 1937; Hastings et al., 2005), in which r is the intrinsic growth rate and D is the diffusion coefficient, to calculate the dispersal phenotype necessary to produce an expansion wave exactly matching the speed of climate change in our simulations (see the model description in Appendix A). This estimated dispersal phenotype matched the observed threshold value distinguishing surviving from extinct populations in all experimental scenarios (Figures B9-B11, vertical dashed line). Thus, surviving populations in each scenario happened to be the lucky few already composed primarily of individuals with dispersal phenotypes capable of spreading at the pace of climate change, rather than populations in which heightened dispersal evolved over time in

response to climate change. However, this threshold effect weakened slightly in scenarios with a

slow speed of climate change, indicating a potential role for dispersal evolution if the climate were

to change at a slow enough rate (Figure B11).

Discussion

Range shifts due to climate change represent a global threat to biodiversity and much recent research has focused on exploring the underlying ecological and evolutionary dynamics of such range shifts to inform conservation efforts. We developed an individual-based model to explore the eco-evolutionary dynamics of climate-induced range shifts in sexually reproducing, diploid populations with both dispersal and environmental niche traits defined by multiple loci. In contrast, previous models have focused on a subset of these factors: ecological dynamics (e.g. (Brooker et al., 2007)), evolution in a single trait only (e.g. (Atkins and Travis, 2010; Henry et al., 2013)), and relatively simple genetic scenarios (e.g. single-locus haploid genetics in asexual populations (Boeye et al., 2013; Hargreaves et al., 2015)). Here, we tested the generality of previous results predicting an important role for dispersal evolution in range shifts (Boeye et al., 2013; Henry et al., 2013) and the interplay of eco-evolutionary dynamics under increased levels of biological complexity. Specifically, we demonstrated the role of spatial population structure, driven by a niche optimum gradient and range edge starkness, in determining extinction risk for range shifting populations via impacts on the equilibrium distribution of dispersal phenotypes and environmental niche values.

Our results suggest that populations characterized by local adaptation to a spatially varying trait optimum and by stark range edges will be less able to track changing climatic conditions (Fig. 2). A survey of the scientific literature found evidence for local adaption in approximately 71% of studies, suggesting a high prevalence of local adaptation in natural populations (Hereford, 2009). While it is difficult to exactly map adaptation to the niche optimum gradient to empirical measures

12

of local adaptation, the parameters defining the steepest gradient used here resulted in the intrinsic formation of stable range boundaries, as seen in previous theoretical studies (Alleaume-Benharira et al., 2006; Kirkpatrick and Barton, 1997; Polechova, 2018; Polechová and Barton, 2015), suggesting they provide reasonable approximations of empirical patterns. Further, a recent meta-analysis of 1400 bird, mammal, fish, and tree species found no evidence for consistent declines in abundance towards range edges (Dallas et al., 2017), suggesting many species exhibit similar abundances at the edge and center of their ranges similar to the starkest range edges imposed in our study. While some of these patterns could represent a publication bias, for example against negative results in studies of local adaptation, combined with our results they suggest many species will face elevated extinction risks in climate-induced range shifts due to their spatial population structure.

Our results emphasize the importance of the equilibrium distribution of dispersal phenotypes (i.e. prior to the onset of rapid climate change) in determining a population's extinction risk during climate change (Fig. 3c&d). Populations primarily composed of high dispersal phenotypes at equilibrium successfully tracked changing climate conditions, while populations of lower dispersal phenotypes lagged behind the changing conditions to eventually go extinct. Importantly, the threshold dividing the equilibrium dispersal phenotypes of successful and extinct populations was constant across all scenarios for a given speed of climate change (Fig. B9-11). Thus, the difference in survival probability among scenarios was driven by the effects of the niche optimum gradient and range edge starkness on the evolution of dispersal ability throughout the range. Scenarios with a steep niche optimum gradient selected for lower dispersal phenotypes at equilibrium due to the potential mismatch of dispersing individuals' niche phenotype and their new location (Kirkpatrick and Barton, 1997). Similarly, a stark range edge selected for lower dispersal due to the risk of dispersing into unsuitable habitat (Shaw et al., 2019, 2014). Previous research has documented a similar reduction in dispersal phenotypes due to an explicit mortality cost of dispersal (Kubisch

13

et al., 2013), whereas the costs to dispersal in our model result from the niche optimum gradient and range edge starkness. Such a cost to dispersal results in lower dispersal phenotypes at equilibrium, hampering a population's ability to successfully track a changing climate. Importantly, dispersal evolution during climate change was unable to counter the influence of equilibrium spatial population structure on extinction dynamics.

While high dispersal phenotypes at equilibrium increased the probability that populations tracked changing conditions, they had the additional effect of reducing average fitness at the range edges when the niche optimum varied through space (Fig. B3-B5). In the model, range edge populations tended to have lower abundance than core populations, increasing their susceptibility to gene flow from the core (García-Ramos and Kirkpatrick, 1997; Kirkpatrick and Barton, 1997). Thus, in populations with high dispersal phenotypes at equilibrium, increased gene flow from the core reduced fitness at the range edge via gene swamping (Lenormand, 2002). As a result, the populations most likely to survive climate change were, counterintuitively, also those characterized by lower fitness at the range edges at equilibrium. While not all populations are characterized by small populations at the range edges (Dallas et al., 2017), our results suggest that high fitness in edge populations may be a warning sign of future difficulty in tracking climate change when the population is structured along a spatial gradient in a trait optimum. For the purposes of this investigation, we assumed the niche optima shifted spatially with climate change, as would be expected if the niche optima corresponded to local temperature or precipitation conditions (Davis and Shaw, 2001). However, in systems characterized by a niche optimum gradient defined by other factors (e.g. geography or biotic interactions) the gradient might remain stable or even shift in an opposing direction to climate change. Future research should investigate the impact of a niche optimum gradient unrelated to climate on extinction risk during range shifts.

Previous research has suggested that evolution of increased dispersal ability during climate

14

change may be capable of rescuing populations that would otherwise be unable to keep pace with shifting environmental conditions (Boeye et al., 2013; Henry et al., 2013). Our results suggest this is not always the case. In fact, it may only be possible under certain, relatively narrow conditions. Previous models showing that dispersal evolution may rescue range shifting populations have typically used relatively simple genetic frameworks to model dispersal, including haploid genetics with a single-locus defining dispersal (Boeye et al., 2013; Hargreaves et al., 2015). As dispersal evolution during range expansions and shifts occurs via the spatial sorting of dispersal alleles throughout the range (Shine et al., 2011), such simplified genetic frameworks may allow more efficient sorting of such alleles compared to situations with more complex genetic structure underlying the dispersal trait. Additionally, the interaction of mutation and genetic architecture in different models (e.g. few mutations of large effects or many mutations of small effects) undoubtedly plays a role in dispersal evolution during range shifts. Increasing mutation rate or effect size might have the equivalent effect of a slower speed of climate change in allowing dispersal evolution to play a greater role in range shift dynamics. Further, life history has been shown to impact the maintenance of genetic diversity, and hence evolutionary potential, with stage and age-structured populations shown to harbor greater diversity then populations with non-overlapping generations as modeled here (Ellner, 1996). Populations defined by more complex life histories might, therefore, contain more genetic diversity in dispersal at equilibrium, making evolution of increased dispersal during range shifts more likely. Thus, further research is needed to understand how factors such as genetic architecture, mutational dynamics, and life history might interact to shape the potential for population rescue via dispersal evolution during range shifts.

15

Conclusion

As climate change continues to threaten populations, communities, and ecosystems (Chen et al., 2011; Gonzalez et al., 2010; Hobbs et al., 2009), it is increasingly important to understand population responses to changing environmental conditions. In particular, a deeper, process-based understanding of extinction risk in range shifting populations will, in turn, allow more focused conservation interventions. Our results suggest that spatial population structure, as determined by the niche optimum gradient and range edge starkness, has the potential to dramatically alter extinction risk for species responding to climate change. Further, in contrast to other studies assuming more simplified genetic architecture, we find very little role for the evolution of heightened dispersal in allowing a population to successfully track climate change. Future work should continue to examine the circumstances determining the potential for rescue via dispersal evolution in range shifts. As climate change continues to accelerate (Chen et al., 2017), it is imperative to identify those factors leading to increased extinction risk in range shifting populations, and use that knowledge to develop meaningful conservation strategies to mitigate such risk.

Appendix A: Full model description

Model overview

Purpose

This model tested an evolving population's ability to track a changing climate under a variety of conditions. Specifically, populations were simulated under different combinations of (1) the slope of the niche optimum gradient and (2) the starkness of the range edge. In all simulations, an individual's expected dispersal distance and environmental niche were defined by an explicit set of quantitative diploid loci subject to mutation, thus allowing both traits to evolve over time. All simulations began with stable climate conditions for 2000 generations to allow the populations to reach a spatial equilibrium before the onset of climate change. Climate change was then modeled as a constant, directional shift in environmental conditions (see *Submodels* below). Finally, simulations ended with another short period of climate stability to assess a population's ability to persist and recover after shifting its range.

State variables and scales

The model simulated a population of males and females characterized by diploid loci for both their expected dispersal distance and environmental niche. Space was modeled as a lattice of discrete patches overlaying a continuous Cartesian coordinate system. Landscapes were two dimensional with a fixed width along the *y* dimension and without bounds on the *x* dimension. Environmental conditions varied along the *x* dimension but remained constant within the *y* dimension. To avoid edge effects due to the fixed width of the *y* dimension, the model employed wrapping boundaries such that if an individual dispersed out of the landscape on one side, it would appear at opposite

17

side of the *y* dimension, but at the same *x* coordinate. Patches were defined by the location of the patch center in *x* and *y* coordinates and a patch width parameter defining the relationship between continuous Cartesian space and the discrete patches used for population dynamics (*Submodels*).

The model implemented climate change by shifting the location of patch carrying capacities and the niche optimum gradient along the *x* dimension of the landscape. Patch carrying capacities were defined by the location of the range center along the *x* dimension, the starkness of the decline characterizing the range edges, and the width of the range along the *x* dimension (See Figure A1). The niche optimum gradient was linear and shifted at the same speed and in the same direction as carrying capacities during climate change.

[Figure A1 goes here]

Process overview and scheduling

Time was modeled in discrete intervals defining single generations of the population (Fig. A2). Within each generation, individuals first dispersed from their natal patches according to their phenotypes. After dispersal, reproduction occurred via a stochastic implementation of the classic Ricker model (Ricker, 1954) taking into account the mean fitness of individuals within the patch. Reproduction occurred via random sampling of the local population (with replacement) weighted by individual relative fitness such that individuals with high relative fitness (as determined by the match between their environmental niche and local conditions) were likely to produce multiple offspring while individuals with low relative fitness might not produce any. Individuals inherited one allele from each parent at each loci, assuming independent segregation and a mutation process. After reproduction, all individuals in the current generation perished and the offspring began the next generation with dispersal, resulting in discrete, non-overlapping generations.

[Figure A2 goes here]

18

Design concepts

Emergence

Emergent phenomena in this model included the spatial distribution of population abundance, dispersal abilities, and relative fitness throughout the range (i.e. the spatial population structure). Additionally, the population dynamics during the range shift, including the extinction process, and the evolutionary trajectories of the dispersal and niche traits were all emergent phenomena in this model.

Stochasticity

All biological processes in this model were stochastic, including realized population growth in each patch, dispersal distances of each individual, and inheritance of loci. Environmental parameters were fixed, however, and the process of climate change (i.e. the movement of patch carrying capacity through time) was deterministic. Thus, the model removed the confounding influence of environmental stochasticity to focus on demographic and evolutionary dynamics of range shifts.

Interactions

Individuals in the model interacted via mating and density-dependent competition within patches. Additionally, the evolutionary trajectories of the two different traits had the potential to interact via the relationship between gene flow (dispersal trait) and local adaptation (niche trait). Further, the niche optimum gradient and range edge starkness could interact with trait evolution both during stable climate conditions and during climate change.

19

Desired output

After each model run, full details of all surviving individuals at the last time point were recorded (spatial coordinates and loci values for both traits). If a population went extinct during the model

run, the time of extinction was recorded. For each occupied patch throughout the simulation, we aggregated data on population size, the dispersal trait, and adaptation to local conditions.

Details

Initialization

The following parameters were set at the beginning of each simulation and formed the initial conditions of the model: the mean and variance for allele values of each trait, initial population size,

location of the range center, number of generations for the pre-, post-, and rapid climate change periods of the simulation, and all other necessary parameters for the submodels defined below. Simulated populations were initialized in the center of the range and allowed to spread and equi-

librate throughout the range during the period of stable climate conditions. This ensured that the populations reacting to a changing climate truly represented the expected spatial distribution for a given range, rather than the initial parameter values used in the simulation (Table A1). Initial

population size was chosen to minimize the risk of stochastic extinction in the early stages of the simulation. The time frames defining climate change were designed to give a reasonable period for the population to reach a spatial equilibrium and a long enough period of climate change for ex-

tinction dynamics to play out. The number of patches defining the *y* dimension and the relationship between Cartesian space and discrete patches were chosen to allow a reasonable number of patches to contribute to the eco-evolutionary dynamics of range shifts while not proving computationally

restrictive.

Submodels

Patch carrying capacities. Patch carrying capacity (K_x) varied along the x dimension of the land-scape, attaining its highest value at the range center and declining with distance from the center. Specifically, the carrying capacity at a location x was defined as the product of the maximum potential carrying capacity (K_{max}) and a function $f(x,t)$, where $f(x,t)$ was bounded between 1 and 0 with its highest value corresponding to the range center. $f(x,t)$ was defined as

$$f(x,t) = \begin{cases} \frac{e^{\gamma(x-\beta_t+\tau)}}{1+e^{\gamma(x-\beta_t+\tau)}} & x \le \beta_t \\ \frac{e^{-\gamma(x-\beta_t-\tau)}}{1+e^{-\gamma(x-\beta_t-\tau)}} & x > \beta_t \end{cases} \tag{A1}$$

where β_t defined the center of the range at time t, τ affected the width of the range, and γ affected the slope of the function at the range edges (See Figure A1). Population dynamics occurred within discrete patches, so to calculate a K_x value for a discrete patch from the continuous function $f(x,t)$, we used another parameter defining the spatial scale of each patch (η). The local carrying capacity of a patch centered on x (K_x) was then calculated as the mean of $f(x,t)$ over the interval of the patch multiplied by K_{max}.

$$K_x = \frac{K_{max}}{\eta} \int_{x-\frac{\eta}{2}}^{x+\frac{\eta}{2}} f(x,t)dx \tag{A2}$$

To understand the relationship between γ and the slope of $f(x,t)$ at the range edge, we calculated the partial derivative of $f(x,t)$ over the x dimension as

$$\frac{\partial f(x,t)}{\partial x} = \begin{cases} \frac{\gamma e^{\gamma(x-\beta_t+\tau)}}{(1+e^{\gamma(x-\beta_t+\tau)})^2} & x \le \beta_t \\ \frac{-\gamma e^{-\gamma(x-\beta_t-\tau)}}{(1+e^{-\gamma(x-\beta_t-\tau)})^2} & x > \beta_t \end{cases} \tag{A3}$$

yielding a value of $\pm\frac{\gamma}{4}$ at the inflection points on either side of the range center ($x = \beta_t \pm \tau$). Thus, altering γ directly altered the range edge starkness. However, changing γ also changed the total

21

Parameter	Description	Value
N_1	Initial population size (seeded across multiple patches) when beginning the simulations	2500 individuals
β_1	Center of the range during stable climate conditions	0
$\hat{t}$	Duration of stable climate conditions	2000 generations
t_Δ	Duration of climate change	100 generations
t_{max}	Total number of generations in the simulation	2150 generations
η	Width of square habitat patches in Cartesian space	50
y_{max}	Number of patches the discrete lattice extends in the y dimension	10 patches

Table A1: Values and descriptions for parameters determining the initial conditions of simulations, the timing of climate change, and the relationship between Cartesian space and the lattice of discrete habitat patches.

area under $f(x,t)$ as can be seen in the indefinite integral of $f(x,t)$:

$$\int_{-\infty}^{\infty} f(x,t)dx = \frac{2ln(e^{\gamma\tau}+1)}{\gamma} \tag{A4}$$

Thus, ranges defined by different γ values could also result in different range-wide carrying ca-
pacities, potentially altering both the ecological (e.g. through stochastic extinction events) and evolutionary (e.g. through more mutations arising in larger populations) dynamics of the ranges. Additionally, different combinations of γ and τ could result in different range widths, which have been shown to impact dispersal evolution within the ranges (Van Kirk and Lewis, 1997). To control for these confounding factors, we fixed the range widths for all scenarios and altered K_{max} to maintain a constant range-wide carrying capacity. Specifically, we defined the range width using the x coordinates at which $f(x,t)$ fell below 0.1 on either side of β_t and chose τ and γ values for each scenario such that $f(x,t)$ fell below 0.1 at the same x coordinates (Table A2). We then adjusted K_{max} for each scenario so that the range-wide carrying capacity was constant (Fig. A3).

[Figure A3 goes here]

Thus, γ and τ were both fixed within a given simulation and β_t (the location of the range center) was used to simulate climate change. During the periods before and after climate change β_t was constant, but to simulate climate change it varied with time as follows

$$\beta_t = v\eta(t-\hat{t}) \tag{A5}$$

where v was the velocity of climate change per generation in terms of discrete patches, t was the current generation, and $\hat{t}$ was the last generation of stable climatic conditions before the onset of climate change.

Niche optimum. The niche optimum ($z_{opt,x}$) varied in space according to

$$z_{opt,x} = \lambda(x-\beta_t) \tag{A6}$$

23

Range edge starkness	Niche optimum gradient	γ	τ	λ	K_{max}
	Flat	0.0025	-240	0	240
Shallow	Shallow	0.0025	-240	0.004	240
	Steep	0.0025	-240	0.008	240
	Flat	0.0075	345.9	0	118.1
Moderate	Shallow	0.0075	345.9	0.004	118.1
	Steep	0.0075	345.9	0.008	118.1
	Flat	0.25	630.1	0	66.7
Stark	Shallow	0.25	630.1	0.004	66.7
	Steep	0.25	630.1	0.008	66.7

Table A2: Descriptions and parameter values for the 9 different experimental scenarios. As defined in the text, γ affects range edge starkness, τ affects the range width, λ is the slope of the niche optimum gradient, and K_{max} is the maximum carrying capacity for patches in the landscape.

with λ determining the rate of change in the optimum across the range. Individual relative fitness ($w_{i,x}$) values were then calculated according to the following equation assuming stabilizing selection

$$w_{i,x} = e^{\frac{-(z_i - z_{opt,x})^2}{2\omega^2}} \tag{A7}$$

where ω defined the strength of stabilizing selection and z_i was an individual's niche phenotype (Lande, 1976). Thus, an individual's realized fitness was higher the closer its niche phenotype (z_i) was to the environmental optimum of the patch it occupied ($z_{opt,x}$). All loci were assumed to contribute additively to an individual's niche value with no dominance or epistasis, meaning an individual's phenotype was simply the sum of the individual's allele values. As defined above, $z_{opt,x}$ also shifted with climate change (i.e. with β_t) as would be expected if it corresponded to a phenotypic optimum along a temperature or precipitation gradient within the range (Davis and Shaw, 2001).

Population dynamics.   Population growth within each patch was modeled with a stochastic implementation of the classic Ricker model (Melbourne and Hastings, 2008; Ricker, 1954). To account for fitness effects on population growth, expected population growth was scaled by the mean relative fitness of individuals within the patch ($\bar{w}_x$) so that maladaptation resulted in reduced population growth. The expected number of new offspring in patch x at time $t + 1$ was given by

$$\hat{N}_{t+1,x} = \bar{w}_x F_{t,x} \frac{R}{\psi} e^{\frac{-RN_{t,x}}{K_x}} \tag{A8}$$

where $F_{t,x}$ was the number of females in patch x at time t, R was the intrinsic growth rate for the population and remained constant in both time and space, ψ was the expected sex ratio of the population, $N_{t,x}$ was the number of individuals (males and females) in patch x at time t, and K_x was the local carrying capacity based on the environmental conditions. To incorporate demographic

Parameter	Description	Value
R	Intrinsic growth rate of the population	2
ψ	Expected sex ratio (proportion of females) in the population	0.5
$\hat{d}$	Maximum achievable dispersal phenotype	1000
ρ	Determines the slope of the transition in dispersal phenotypes from 0 to D	0.5

Table A3: Values and descriptions for parameters related to population growth and dispersal.

stochasticity, the realized number of offspring for each patch was then drawn from a Poisson distribution.

$$N_{t+1,x} \sim Poisson(\hat{N}_{t+1,x}) \tag{A9}$$

Offspring parentage was assigned by random sampling of the local male and female populations (i.e. polygynandrous mating assuming a well-mixed population within each patch). The sampling was weighted by individual fitness and occurred with replacement so highly fit individuals were likely to have multiple offspring while low fitness individuals might not have had any. Each offspring inherited one allele per locus from each parent, assuming no linkage among loci. After reproduction, all members of the previous generation died and the offspring dispersed to begin the next generation. Parameters governing population dynamics (Table A3) were chosen to yield reasonable rates of population growth based on initial exploratory simulations.

Mutation. Inherited alleles were subject to mutation such that some offspring might not inherit identical copies of certain alleles from their parents. The mutation process was defined by two parameters for each trait T: the diploid mutation rate (U^T) and the mutational variance (V_m^T). Using these parameters along with the number of loci defining trait T (L^T), the per locus probability of a mutation was

$$\frac{U^T}{2L^T} \tag{A10}$$

Effect sizes of mutations were drawn from a normal distribution with mean 0 and a standard deviation of

$$\sqrt{V_m^T U^T} \tag{A11}$$

meaning the ratio of small effect to large effect mutations depended on both U^T and V_m^T. We chose parameter values (Table A4) in keeping with previously derived values from the literature (Gilbert et al., 2017). For the number of loci used in our simulations, these resulted in mostly mutations of small effect with few large effect mutations. Importantly, by defining the mutation process in this way, rather than with a per locus probability of mutation and a mutation effect size directly, the mutational input per generation was kept constant regardless of the number of loci defining the trait (Schiffers et al., 2014).

Dispersal. Finally, individuals dispersed according to an exponential dispersal kernel defined by each individual's dispersal phenotype. An individual's dispersal phenotype was the expected dispersal distance and was given by

$$d_i = \frac{\hat{d}\eta e^{\rho \Sigma L^D}}{1 + e^{\rho \Sigma L^D}} \tag{A12}$$

where $\hat{d}$ was the maximum expected dispersal distance in terms of discrete patches, ρ was a constant determining the slope of the transition between 0 and $\hat{d}$, and the summation was taken across

Parameter	Description	Value
ω	Defines the strength of stabilizing selection on fitness traits	3
U^T	Diploid mutation rate for each trait	0.02
V_m^T	Mutational variance for each trait	0.0004
L^T	Number of diploid loci defining each trait	5 loci
μ_1^f	Initial mean allele value for the niche trait	0
μ_1^d	Initial mean allele value for the dispersal trait	-1
σ_1^f	Initial standard deviation of allele values for the niche trait	0.025
σ_1^d	Initial standard deviation of allele values for the dispersal trait	1

Table A4: Values and descriptions for parameters defining the genetic components of the model.

all alleles contributing to dispersal. Thus, as with fitness, loci were assumed to contribute addi-
tively with no dominance or epistasis. The expected dispersal distance, d_i was then used to draw
a realized distance from an exponential dispersal kernel. The direction of dispersal (in radians)
was drawn from a uniform distribution bounded by 0 and 2π. If a dispersal trajectory took an
individual outside the bounds of the landscape in the *y* dimension, the individual reappeared at the
same *x* coordinate but the opposite end of the *y* dimension, thus wrapping the top and bottom edges
of the landscape to avoid edge effects. Dispersal occurred from the center of each patch and the
individual's new patch was then determined according to its location in the overlaid grid of η x η
patches (see Figure A1). Dispersal parameters (Table A3) were chosen to allow a wide range of
dispersal phenotypes to evolve in the context of the different experimental scenarios, ranging from
highly restrictive to long-distance dispersal.

Since the dispersal phenotype was the expected value of the exponential dispersal kernel, it
could be used directly to calculate the two-dimensional diffusion coefficient of population spread
(*D*). Specifically, since d_i^2 represented the mean squared displacement of an individual with dis-
persal phenotype d_i, the two-dimensional diffusion coefficient could be calculated as

$$D = \frac{1}{4}d_i^2 \qquad \text{(A13)}$$

and subsequently used to calculate the approximate speed of an expansion wave defined by that
dispersal phenotype.

Appendix B: Supplementary results for varying speeds of climate change

Extinction probability

As in the main text, we calculated the cumulative probability of extinction for both slow and fast speeds of climate change. The figures in this section use the same layout and line types as Figure 2 in the main text to allow for direct comparisons.

[Figures B1&B2 go here.]

Equilibrium fitness throughout the landscape

To assess trends in realized fitness values throughout the landscape, we calculated patch-level mean individual fitness for each landscape at equilibrium. To simplify the figures, we averaged over the y dimension in which the CV in niche genotypes was minimal throughout the range for all scenarios (typically below 0.25) due to the constant environmental conditions. Populations at the range edge were characterized by reduced fitness compared to core populations, as found in previous models (García-Ramos and Kirkpatrick, 1997). However, this trend was exacerbated in populations that successfully tracked climate change compared to those that went extinct, especially in the presence of gradual range edges and steep niche optimum gradients. As realized fitness values do not vary spatially in simulations with no gradient in the niche optimum, the following figures only show results for scenarios with a shallow or steep gradient.

[Figures B3-B5 go here.]

30

Dispersal evolution

Using the same metric of dispersal evolution from the main text (change in average phenotype for each patch), we display here the observed dispersal evolution over the course of climate change for all experimental scenarios. Each histogram in the following figures represents a single experimental scenario as indicated by the figure text. The lower left panel and upper right panel from Figure B7 are the same histograms shown in Figure 3a&b, but are here placed in the context of all other experimental scenarios.

[Figures B6-B8 go here.]

Equilibrium dispersal phenotypes

Here, we present histograms of the equilibrium distribution of dispersal phenotypes to demonstrate the importance of those phenotypes in determining population success or extinction during climate change. Dispersal phenotypes are log transformed for easier comparison. As with the dispersal evolution section, each histogram represents a single experimental scenario as indicated by the figure text. Similarly, the lower left panel and upper right panel from Figure B10 are the same histograms shown in Figure 3c&d, but are here placed in the context of all other experimental scenarios. All histograms additionally have a vertical dashed line indicating the dispersal phenotype necessary to produce an expansion wave traveling at exactly the speed of climate change in each simulation. This value serves as a threshold to distinguish individuals from ultimately successful versus extinct populations.

[Figures B9-B11 go here.]

31

Literature Cited

Aguilée, R., G. Raoul, F. Rousset, and O. Ronce. 2016. Pollen dispersal slows geographical range shift and accelerates ecological niche shift under climate change. Proceedings of the National Academy of Sciences 113:E5741–E5748.

Alleaume-Benharira, M., I. Pen, and O. Ronce. 2006. Geographical patterns of adaptation within a species? range: interactions between drift and gene flow. Journal of evolutionary biology 19:203–215.

Atkins, K., and J. Travis. 2010. Local adaptation and the evolution of species' ranges under climate change. Journal of Theoretical Biology 266:449–457.

Bocedi, G., S. C. Palmer, G. Pe'er, R. K. Heikkinen, Y. G. Matsinos, K. Watts, and J. M. Travis. 2014. Rangeshifter: a platform for modelling spatial eco-evolutionary dynamics and species' responses to environmental changes. Methods in Ecology and Evolution 5:388–396.

Boeye, J., J. M. Travis, R. Stoks, and D. Bonte. 2013. More rapid climate change promotes evolutionary rescue through selection for increased dispersal distance. Evolutionary Applications 6:353–364.

Brooker, R. W., J. M. Travis, E. J. Clark, and C. Dytham. 2007. Modelling species' range shifts in a changing climate: the impacts of biotic interactions, dispersal distance and the rate of climate change. Journal of Theoretical Biology 245:59–65.

Case, T. J., and M. L. Taper. 2000. Interspecific competition, environmental gradients, gene flow, and the coevolution of species' borders. The American Naturalist 155:583–605.

Chen, I.-C., J. K. Hill, R. Ohlemüller, D. B. Roy, and C. D. Thomas. 2011. Rapid range shifts of species associated with high levels of climate warming. Science 333:1024–1026.

Chen, X., X. Zhang, J. A. Church, C. S. Watson, M. A. King, D. Monselesan, B. Legresy, and C. Harig. 2017. The increasing rate of global mean sea-level rise during 1993–2014. Nature Climate Change 7:492.

Dallas, T., R. R. Decker, and A. Hastings. 2017. Species are not most abundant in the centre of their geographic range or climatic niche. Ecology Letters 20:1526–1533.

Davis, M. B., and R. G. Shaw. 2001. Range shifts and adaptive responses to quaternary climate change. Science 292:673–679.

Ellner, S. 1996. Environmental fluctuations and the maintenance of genetic diversity in age or stage-structured populations. Bulletin of Mathematical Biology 58:103–127.

Excoffier, L., M. Foll, and R. J. Petit. 2009. Genetic consequences of range expansions. Annual Review of Ecology, Evolution, and Systematics 40:481–501.

Fisher, R. A. 1937. The wave of advance of advantageous genes. Annals of eugenics 7:355–369.

García-Ramos, G., and M. Kirkpatrick. 1997. Genetic models of adaptation and gene flow in peripheral populations. Evolution 51:21–28.

Gilbert, K. J., N. P. Sharp, A. L. Angert, G. L. Conte, J. A. Draghi, F. Guillaume, A. L. Hargreaves, R. Matthey-Doret, and M. C. Whitlock. 2017. Local adaptation interacts with expansion load during range expansion: Maladaptation reduces expansion load. The American Naturalist 189:368–380.

33

Gonzalez, P., R. P. Neilson, J. M. Lenihan, and R. J. Drapek. 2010. Global patterns in the vulnerability of ecosystems to vegetation shifts due to climate change. Global Ecology and Biogeography 19:755–768.

Grimm, V., U. Berger, D. L. DeAngelis, J. G. Polhill, J. Giske, and S. F. Railsback. 2010. The odd protocol: a review and first update. Ecological Modelling 221:2760–2768.

Hargreaves, A., S. Bailey, and R. A. Laird. 2015. Fitness declines towards range limits and local adaptation to climate affect dispersal evolution during climate-induced range shifts. Journal of Evolutionary Biology 28:1489–1501.

Hargreaves, A. L., and C. G. Eckert. 2014. Evolution of dispersal and mating systems along geographic gradients: implications for shifting ranges. Functional Ecology 28:5–21.

Hastings, A., K. Cuddington, K. F. Davies, C. J. Dugaw, S. Elmendorf, A. Freestone, S. Harrison, M. Holland, J. Lambrinos, U. Malvadkar, et al. 2005. The spatial spread of invasions: new developments in theory and evidence. Ecology Letters 8:91–101.

Henry, R. C., G. Bocedi, and J. M. Travis. 2013. Eco-evolutionary dynamics of range shifts: elastic margins and critical thresholds. Journal of Theoretical Biology 321:1–7.

Hereford, J. 2009. A quantitative survey of local adaptation and fitness trade-offs. The American Naturalist 173:579–588.

Hobbs, R. J., E. Higgs, and J. A. Harris. 2009. Novel ecosystems: implications for conservation and restoration. Trends in Ecology & Evolution 24:599–605.

Holt, R. D., T. H. Keitt, M. A. Lewis, B. A. Maurer, and M. L. Taper. 2005. Theoretical models of species? borders: single species approaches. Oikos 108:18–27.

34

Kirkpatrick, M., and N. H. Barton. 1997. Evolution of a species' range. The American Naturalist 150:1–23.

Kubisch, A., T. Degen, T. Hovestadt, and H. J. Poethke. 2013. Predicting range shifts under global change: the balance between local adaptation and dispersal. Ecography 36:873–882.

Lande, R. 1976. Natural selection and random genetic drift in phenotypic evolution. Evolution 30:314–334.

Lenormand, T. 2002. Gene flow and the limits to natural selection. Trends in Ecology & Evolution 17:183–189.

Loarie, S. R., P. B. Duffy, H. Hamilton, G. P. Asner, C. B. Field, and D. D. Ackerly. 2009. The velocity of climate change. Nature 462:1052.

Melbourne, B. A., and A. Hastings. 2008. Extinction risk depends strongly on factors contributing to stochasticity. Nature 454:100.

Mustin, K., T. G. Benton, C. Dytham, and J. M. Travis. 2009. The dynamics of climate-induced range shifting; perspectives from simulation modelling. Oikos 118:131–137.

Ochocki, B. M., and T. E. Miller. 2017. Rapid evolution of dispersal ability makes biological invasions faster and more variable. Nature Communications 8:14315.

Parmesan, C. 2006. Ecological and evolutionary responses to recent climate change. Annual Review of Ecology, Evolution, and Systematics 37:637–669.

Phillips, B. L. 2015. Evolutionary processes make invasion speed difficult to predict. Biological Invasions 17:1949–1960.

594 Polechova, J. 2018. Is the sky the limit? on the expansion threshold of a species? range. PLoS biology 16:e2005372.

Polechová, J., and N. H. Barton. 2015. Limits to adaptation along environmental gradients. Pro-
597 ceedings of the National Academy of Sciences page 201421515.

Ricker, W. E. 1954. Stock and recruitment. Journal of the Fisheries Board of Canada 11:559–623.

Schiffers, K., F. M. Schurr, J. M. Travis, A. Duputié, V. M. Eckhart, S. Lavergne, G. McInerny,
600 K. A. Moore, P. B. Pearman, W. Thuiller, et al. 2014. Landscape structure and genetic architec-
ture jointly impact rates of niche evolution. Ecography 37:1218–1229.

Sexton, J. P., P. J. McIntyre, A. L. Angert, and K. J. Rice. 2009. Evolution and ecology of species
603 range limits. Annu. Rev. Ecol. Evol. Syst. 40:415–436.

Shaw, A. K., C. C. D?Aloia, and P. M. Buston. 2019. The evolution of marine larval dispersal kernels in spatially structured habitats: Analytical models, individual-based simulations, and
606 comparisons with empirical estimates. The American Naturalist 193:000–000.

Shaw, A. K., M. Jalasvuori, and H. Kokko. 2014. Population-level consequences of risky dispersal. Oikos 123:1003–1013.

609 Shaw, A. K., and H. Kokko. 2015. Dispersal evolution in the presence of allee effects can speed up or slow down invasions. The American Naturalist 185:631–639.

Shine, R., G. P. Brown, and B. L. Phillips. 2011. An evolutionary process that assembles pheno-
612 types through space rather than through time. Proceedings of the National Academy of Sciences 108:5708–5711.

Szűcs, M., M. Vahsen, B. Melbourne, C. Hoover, C. Weiss-Lehman, and R. Hufbauer. 2017. Rapid
adaptive evolution in novel environments acts as an architect of population range expansion.
Proceedings of the National Academy of Sciences 114:13501–13506.

Team, R. C. 2000. R language definition. Vienna, Austria: R Foundation for Statistical Computing
.

Van Kirk, R. W., and M. A. Lewis. 1997. Integrodifference models for persistence in fragmented
habitats. Bulletin of Mathematical Biology 59:107.

Wallace, B. 1975. Hard and soft selection revisited. Evolution 29:465–473.

Weiss-Lehman, C., R. A. Hufbauer, and B. A. Melbourne. 2017. Rapid trait evolution drives in-
creased speed and variance in experimental range expansions. Nature Communications 8:14303.
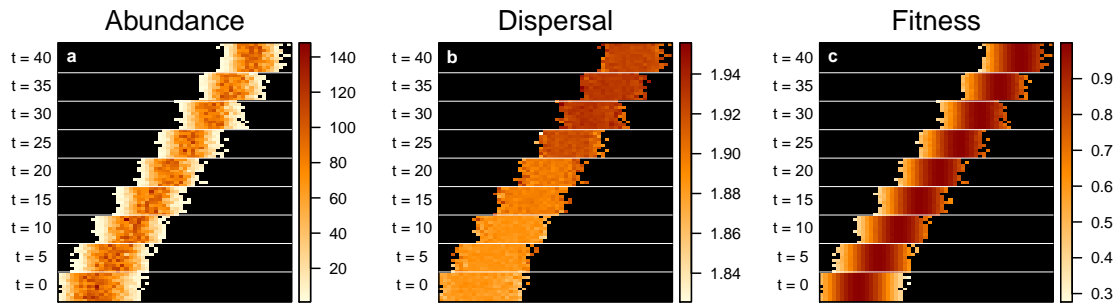
Figures

Figure 1: A single example of a simulation with a steep niche optimum gradient and a moderately stark range edge. Information on the (a) abundance, (b) dispersal ability, and (c) fitness of individuals in each patch is shown for time periods beginning with the last generation of stable climate conditions ($t = 0$) to 40 generations after the start of climate change. Log transformed mean dispersal phenotypes (b) are shown for each patch. Average patch fitness (c) was calculated based on the mean niche trait of local individuals and the niche optimum for each patch.
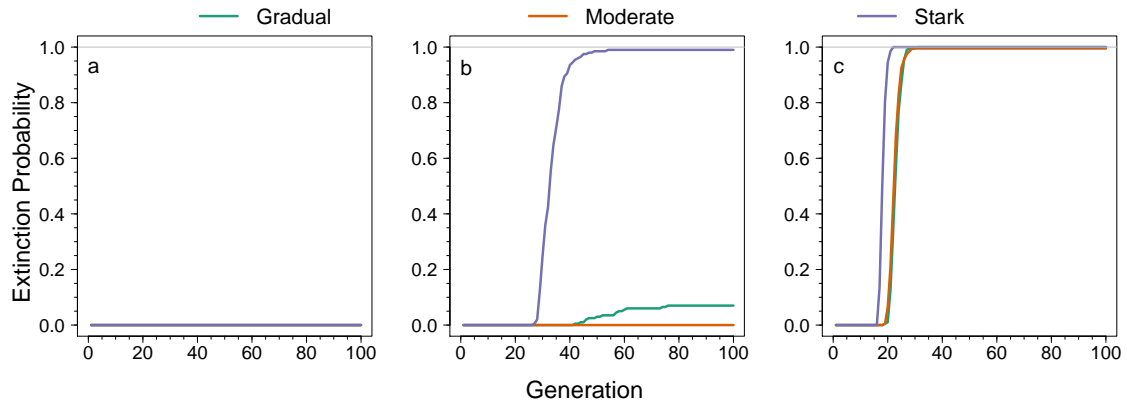
Figure 2: The cumulative probability of extinction due to a moderate speed of climate change in different experimental scenarios. Graphs show the proportion of simulated populations that went extinct through time for scenarios with a (a) flat, (b) shallow, and (c) steep niche optimum gradient, and in ranges characterized by shallow (solid line), moderate (dashed line), or stark (dotted line) edges. In all graphs, a horizontal grey line shows %100 extinction.
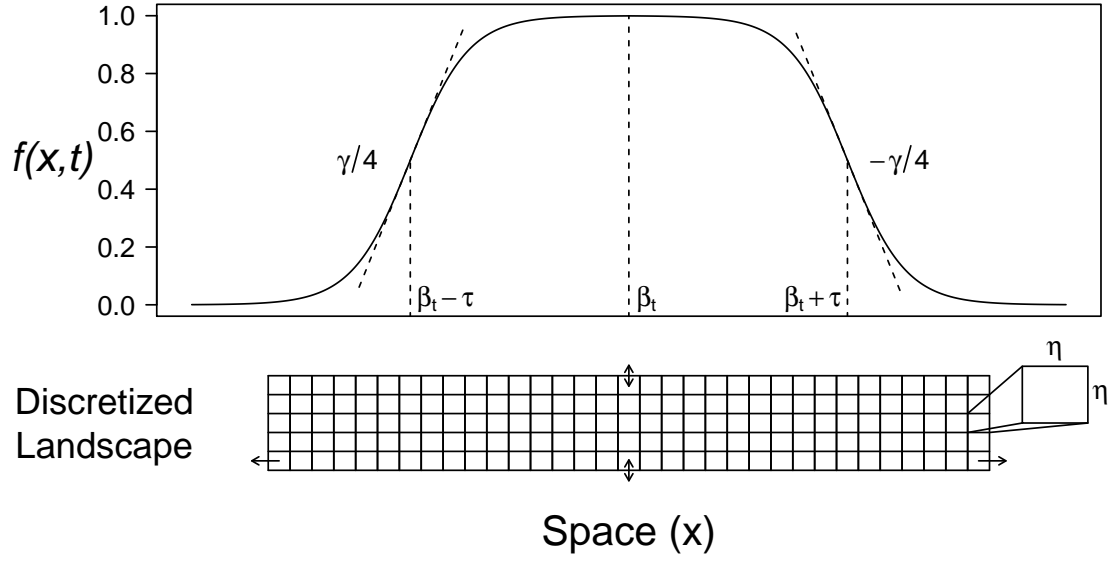
Figure A1: Example visualization of $f(x,t)$ in Cartesian space. The parameters of $f(x,t)$ are shown on the figure at significant points along the x axis. Specifically, β_t defined the range center, γ determined the slope of $f(x,t)$ at the inflection points (i.e. the range edges), and τ determined the location of the inflection points. The lattice of discrete η x η patches in which population dynamics occurred is shown beneath. As described in the *Submodels* section of Appendix A, $f(x,t)$ determined the carrying capacity of the patches along the x dimension of the lattice while carrying capacity remained constant within each column along the y dimension. Landscapes were unbounded in the x dimension and implemented with wrapping boundaries in the y dimension.

(4) Determine the population size for each patch in generation t + 1

REPRODUCTION

(5) Determine which individuals reproduce by random sampling weighted by individual finesses

(3) Assign individuals to discrete patches, defining local populations for subsequent reproduction

DISPERSAL

(6) Offspring inherit alleles from each parent assuming no linkage among loci

(2) Individuals disperse in continuous space assuming an exponential dispersal kernel and unbiased directionality

(1) Calculate dispersal phenotypes for each individual

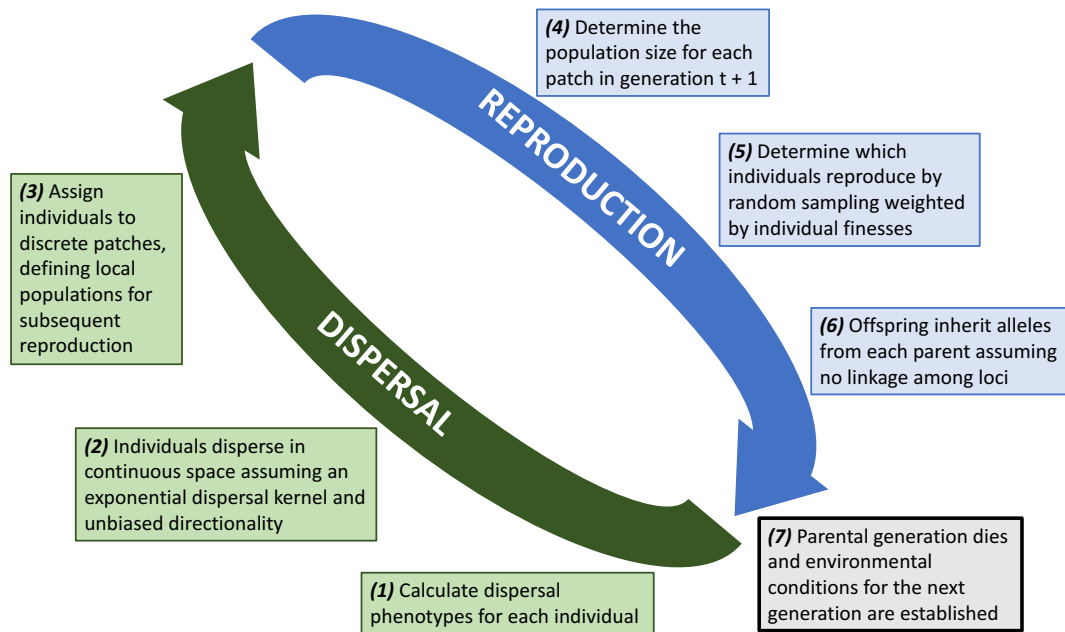**(7)** Parental generation dies and environmental conditions for the next generation are established

Figure A2: The life cycle of simulated populations is shown divided between events contributing to reproduction and dispersal. Each generation began with new offspring dispersing according to their phenotype, after which reproduction occurred in local populations defined by the discrete lattice. After reproduction, all parental individuals perished, resulting in discrete, non-overlapping generations.
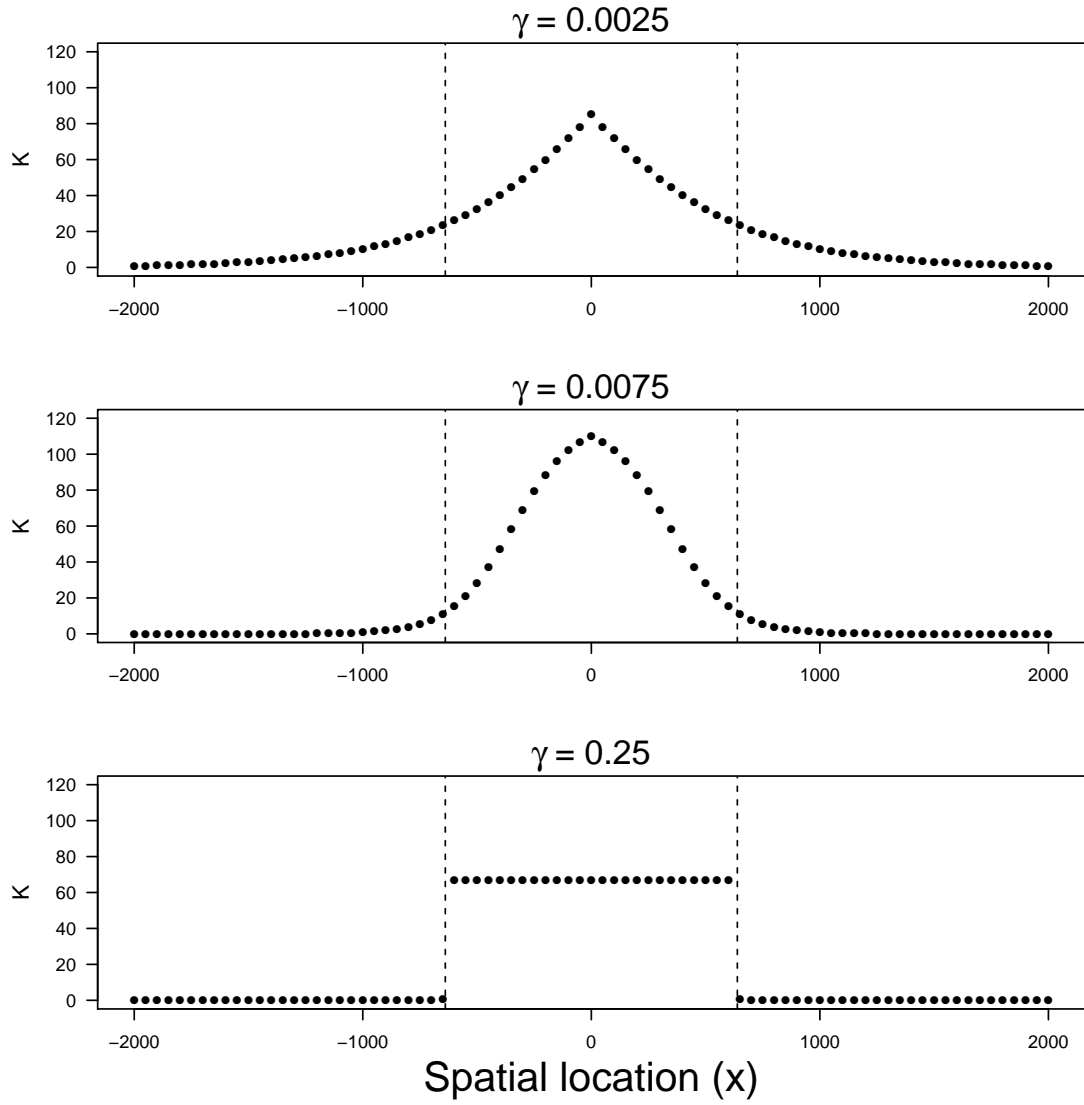
Figure A3: The carrying capacity of discrete patches along the *x* dimension of landscapes. From top to bottom, the plots show the carrying capacities for gradual, moderate, and stark range edges. Points represent the carrying capacity of a discrete η x η patch in the range. The vertical dashed lines indicate the *x* coordinates at which $f(x,t)$ declines below 0.1 and the γ value for each plot is listed above.
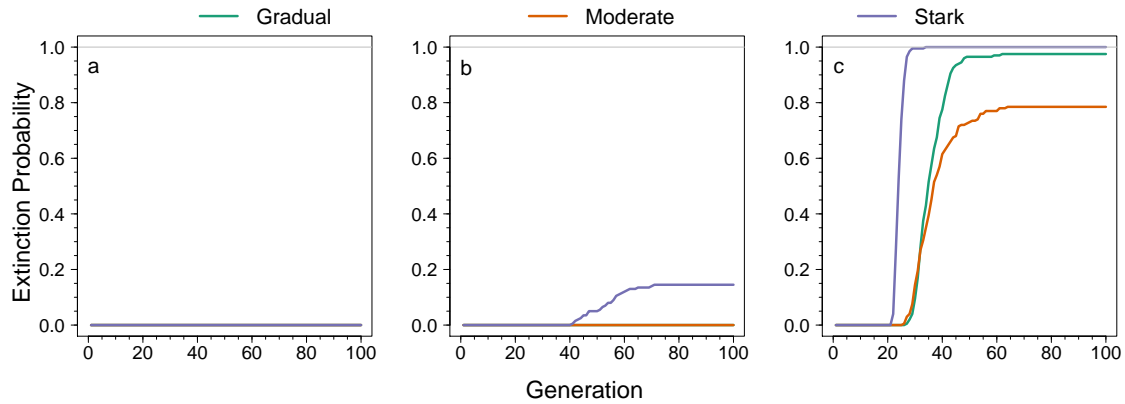
Figure B1: The cumulative probability of extinction due to a slow speed of climate change in different experimental scenarios. Graphs show the proportion of simulated populations that went extinct through time for scenarios with a (a) flat, (b) shallow, and (c) steep niche optimum gradient, and in ranges characterized by a shallow (solid line), moderate (dashed line), or stark (dotted line) edge. In all graphs, a horizontal grey line shows %100 extinction.
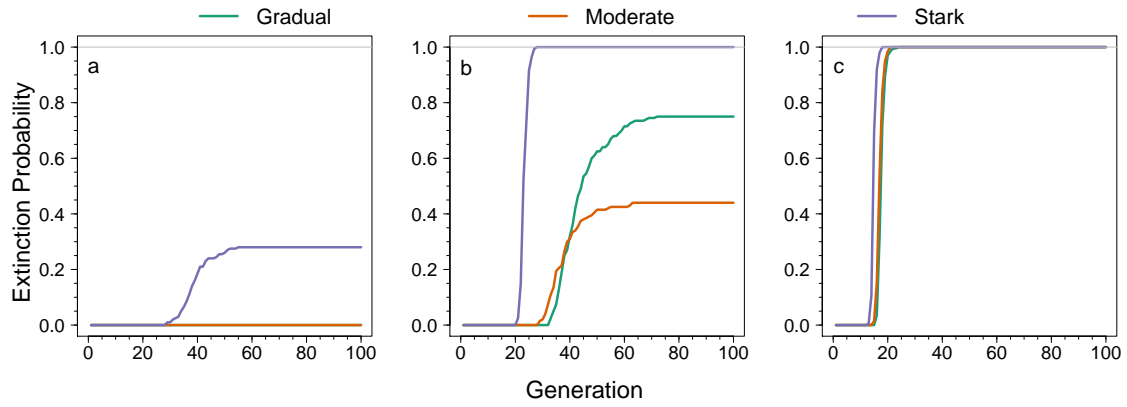
Figure B2: The cumulative probability of extinction due to a fast speed of climate change in different experimental scenarios. Graphs show the proportion of simulated populations that went extinct through time for scenarios with a (a) flat, (b) shallow, and (c) steep niche optimum gradient, and in ranges characterized by a shallow (solid line), moderate (dashed line), or stark (dotted line) edge. In all graphs, a horizontal grey line shows %100 extinction.